Simple Adaptive Control for a Flywheel Zero-Bias AMB System

Yong He, Kenzo Nonami and Zengyi Zhang

Abstract—**The active magnetic bearing (AMB)-flywheel system is used as a storage device for electrical energy, it is desirable to minimize the energy required for its stabilization control. We apply an almost strictly positive real (ASPR)-based simple adaptive control (SAC) scheme to an AMB-flywheel energy storage system using the zero-bias current method. Since most practical systems do not satisfy the ASPR condition, the ASPR conditions are the fundamental restrictions for practical applications of the SAC control. The AMB-flywheel is a multiple-input multiple-output (MIMO) system with five degrees of freedom (DOF). We propose a design method for performing ASPR-augmented control for a MIMO AMB-flywheel system with five degrees of freedom; the method uses a parallel feed forward compensator for MIMO SAC. The SAC controller was proposed for application to an AMB-flywheel system and control performance was improved by combining SAC with a D controller. The SAC-D controller is evaluated via simulations and experiments. We present the analysis of the influence of external disturbances from the EV driving on the road about the AMB-flywheel system. The results demonstrate that the SAC controller can stabilize levitation of the AMB system under real disturbance without any touchdown.**

Keywords—**AMB-Flywheel, Simple Adaptive Control (SAC), Magnetic Levitation and Almost Strictly Positive Realness**

I. INTRODUCTION

In recent times, many world-renowned automobile manufacturers are expending efforts on research and development of energy-efficient hybrid cars and pollution-free electric vehicles. However, the primary factor constraining this development is the battery. Flywheel energy storage is becoming one of the most promising power batteries in electric vehicles.

If Active magnetic bearing (AMB) systems are composed of electromechanical actuators, power amplifiers, controllers, and position sensors that provide contact-free suspension of the rotor. Since friction is absent and lubrication is not needed, contact-free AMBs are especially suitable for flywheel systems.

One of the main drawbacks of an AMB system is that it requires a feedback control using an electromagnetic force to suspend the rotor at the origin in a non-contact condition. Therefore, AMBs require a well-designed control system to remain operational.

The electromagnetic force generated by a magnetic bearing is highly nonlinear. Magnetic bearings with a zero-bias current have the potential to reduce power losses because only a single electromagnet of the pair is operational at any given time [1].

Most adaptive control schemes, including classical model reference adaptive control systems (MRACs), self-tuning regulators (STRs), generalized predictive control (GPC), etc., require that a large number of "tuning knobs" be adjusted prior to the actual commissioning of an adaptive controller [2]. Simple adaptive control (SAC) was developed to counter this criticism. This algorithm is called "simple" because it does not use an identifier or observers in the control loop. It is a simple and robust algorithm for unmodeled dynamics since the order of the reference model can be chosen almost freely regardless of that of the controlled system. Harnessing this advantage, our group has proposed an SAC combined with a proportional integral derivative controller method as part of prophase research on an AMB-flywheel system [5]. In this study, a complete SAC controller with a zero-bias method is applied to our AMB-flywheel system to improve the system performance.

To the scheme requires that the plant to be controlled be strictly positive real (SPR) or almost strictly positive real (ASPR). In this study, we apply an ASPR-based SAC scheme to the AMB-flywheel system. It is well known that the introduction of a parallel feedforward compensator (PFC) is considered as one of the most common and useful methods for applying ASPR-based SAC for non-ASPR-controlled systems. Using this control method, we performed some simulations and experiments to analyze the performance of the AMB-flywheel system.

II. MODEL OF AMB FLYWHEEL

Let us consider the magnetic levitation system shown in Fig. 1. This AMB-flywheel was designed as a vertical structure. In this research, it will be installed on the electrical vehicle (EV) as the vertical direction, so we should defined z axis as the

Yong He From 2010 to now, he worked as a Phd. Candidate in Chiba University, Chiba, Japan. His research interests include flywheel energy storage systems, active magnetic bearings, and power quality issues in flywheel energy storage system.

Kenzo Nonami (M'97) received the M.S. and Ph.D. degrees from Tokyo Metropolitan University, Tokyo, Japan, in 1976 and 1979, respectively. He is currently a Professor in the Department of Electronics and Mechanical Engineering, Chiba University, Chiba.

Zengyi Zhang From 2012 to now，he worked as a master. Candidate in Chiba University，Chiba, Japan. His research interests include the stable control methods of active magnetic bearings in flywheel energy storage system

gravity direction in the modeling of it in Fig. 1. The equation of motion of a rigid rotor-active magnetic bearing system in radial direction is derived as:

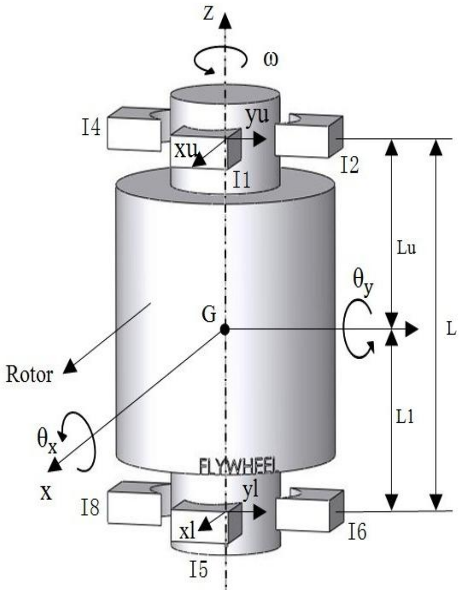

Fig. 1: Model of AMB with flywheel

$$\begin{cases} m\ddot{x} = F_x + m\delta\omega^2 \cos\omega t \\ I_r\ddot{\theta}_y - I_z\omega\dot{\theta}_x = N_y + ml_c\delta\omega^2 \cos\omega t \\ m\ddot{y} = F_y + m\delta\omega^2 \sin\omega t \\ I_r\ddot{\theta}_x + I_z\omega\dot{\theta}_y = N_x + ml_c\delta\omega^2 \sin\omega t \end{cases} \tag{1}$$

Where x and y denote the linear**displacement of the rotor's center of mass along the x and y axes, respectively. Similarly, θ_y and θ_x denote the angular displacements of the rotor around the x and y axes, respectively. F_x and F_y denote the electromagnetic forces acting on the bearing in the x and y directions, respectively. ω denotes the flywheel rotation speed; δ, the eccentricity; m, the mass of the rotor; I_z, the moment of inertia about the z axis; and I_r, the moment of inertia about the x and y axes. N_x and N_y denote the moment of force about the x and y axes, respectively. F_x, F_y, N_x, and N_y can be expressed as:

$$\begin{cases} F_x = f_{xu} + f_{xl}, F_y = f_{yu} + f_{yl} \\ N_x = f_{yl}L_l - f_{yu}L_u, N_y = f_{xu}L_u - f_{xl}L_l \end{cases} \tag{2}$$

The forces at the upper and lower coils of the AMB in the x and y directions are given as:

$$\begin{cases} f_{xu} = \dfrac{K_u i_1^2}{(X_0 - X_u)^2} - \dfrac{K_u i_3^2}{(X_0 + X_u)^2} \\ f_{xl} = \dfrac{K_l i_5^2}{(X_0 - X_l)^2} - \dfrac{K_l i_7^2}{(X_0 + X_l)^2} \\ f_{yu} = \dfrac{K_u i_2^2}{(Y_0 - Y_u)^2} - \dfrac{K_u i_4^2}{(Y_0 + Y_u)^2} \\ f_{yl} = \dfrac{K_l i_6^2}{(Y_0 - Y_l)^2} - \dfrac{K_l i_8^2}{(Y_0 + Y_l)^2} \end{cases} \tag{3}$$

The displacements at the upper and lower coils of the AMB in the x and y directions are given as:

$$\begin{cases} X_u = x + L_u\theta_y, X_l = x - L_l\theta_y \\ Y_u = y - L_u\theta_x, Y_l = y + L_l\theta_x \end{cases} \tag{4}$$

On the basis of the above equations of motion, we choose $x_1 = (x, \theta_y, y, \theta_x)^T$ and $x_2 = (\dot{x}, \dot{\theta}_y, y, \dot{\theta}_x)^T$ as the state variables and $U = (f_{xu}, f_{xl}, f_{yu}, f_{yl})^T$ as the control input; then, the state space equations are given as:

$$\frac{d}{dt}\begin{pmatrix} x_1 \\ x_2 \end{pmatrix} = \begin{pmatrix} O_{4\times4} & I_{4\times4} \\ O_{4\times4} & A_{22} \end{pmatrix}\begin{pmatrix} x_1 \\ x_2 \end{pmatrix} + \begin{pmatrix} O_{4\times4} \\ B_2 \end{pmatrix}U + \begin{pmatrix} O_{4\times2} \\ E_2 \end{pmatrix}\begin{pmatrix} \cos(wt) \\ \sin(wt) \end{pmatrix} \tag{5}$$

$$\begin{pmatrix} X_u \\ X_l \\ Y_u \\ Y_l \end{pmatrix} = \begin{pmatrix} 1 & L_u & 0 & 0 & 0 & 0 & 0 & 0 \\ 1 & -L_l & 0 & 0 & 0 & 0 & 0 & 0 \\ 0 & 0 & 1 & -L_u & 0 & 0 & 0 & 0 \\ 0 & 0 & 1 & L_l & 0 & 0 & 0 & 0 \end{pmatrix}\begin{pmatrix} x_1 \\ x_2 \end{pmatrix} \tag{6}$$

Where

$$A_{22} = \begin{pmatrix} 0 & 0 & 0 & 0 \\ 0 & 0 & 0 & \omega I_Z / I_r \\ 0 & 0 & 0 & 0 \\ 0 & -\omega I_Z / I_r & 0 & 0 \end{pmatrix} \tag{7}$$

$$B_2 = \begin{pmatrix} 1/m & 1/m & 0 & 0 \\ L_u / I_r & -L_l / I_r & 0 & 0 \\ 0 & 0 & 1/m & 1/m \\ 0 & 0 & -L_u / I_r & L_l / I_r \end{pmatrix} \tag{8}$$

$$E_2 = \begin{pmatrix} \delta\omega^2 & 0 \\ ml_c\delta\omega^2 / I_r & 0 \\ 0 & \delta\omega^2 \\ 0 & ml_c\delta\omega^2 / I_r \end{pmatrix} \tag{9}$$

According to (4) above, the conversion relation between state variable $x_1 = (x, \theta_y, y, \theta_x)^T$ and the displacement in the x and y directions can be given as:

$$\begin{pmatrix} x \\ \theta_y \\ y \\ \theta_x \end{pmatrix} = T\begin{pmatrix} X_u \\ X_l \\ Y_u \\ Y_l \end{pmatrix}, \; T = \begin{pmatrix} L_l / L & L_u / L & 0 & 0 \\ 1/L & -1/L & 0 & 0 \\ 0 & 0 & L_l / L & L_u / L \\ 0 & 0 & -1/L & 1/L \end{pmatrix} \tag{10}$$

where $L = L_u + L_l$. Then, the state variable transfer equation can be written as:

$$\begin{pmatrix} x_1 \\ x_2 \end{pmatrix} = GX', \quad G = \begin{pmatrix} T & 0 \\ 0 & T \end{pmatrix} \tag{11}$$

According to the relation equation above, the state space equation of the AMB-flywheel system can be expressed as:

$$\begin{cases} \dot{X}' = \overline{A}X' + \overline{B}U + \overline{E}\begin{pmatrix} \cos(\omega t) \\ \sin(\omega t) \end{pmatrix} \\ \overline{A} = G^{-1}AG, \overline{B} = G^{-1}B, \overline{E} = G^{-1}E \end{cases} \tag{12}$$

where $X' = [x_1', x_2']^T, x_1' = [X_u, X_l, Y_u, Y_l] \quad x_2' = [\dot{X}_u, \dot{X}_l, \dot{Y}_u, \dot{Y}_l]$.

One pair of AMBs is present along the axial direction. If the electromagnetic induction is proportional to the magnetic field and the current is below saturation, then the force is a function of coil current and air gap. The motion equation for this can be written as:

$$m\ddot{z} = F_z - mg \tag{13}$$

$$F_z = k\left(\frac{I_u + i}{z_u - z}\right)^2 - k\left(\frac{I_l - i}{z_l + z}\right)^2 \tag{14}$$

where F_z is the magnetic force generated by the z direction coils. z_u and z_l are the air gaps in the upper and lower coils, respectively, in the axial direction and z is the displacement in the z direction. Further, I_u and I_l are the bias currents in the upper and lower coils, respectively, and i is the control current. From (14), it can be seen that the magnetic bearing has nonlinearity, so we extend this equation around the balance position.

$$m\ddot{z} = k_z z + k_i i + F_0 - mg \tag{15}$$

$$k_z = 2k\left(\frac{I_u^2}{z_u^3} + \frac{I_l^2}{z_l^3}\right), k_i = 2k\left(\frac{I_u}{z_u^2} + \frac{I_l}{z_l^2}\right) \tag{16}$$

$$F_o = k\left(\frac{I_u^2}{z_u^2} - \frac{I_l^2}{z_l^2}\right) \tag{17}$$

The term F_0 in (15) is used to compensate for gravity at the balance position. Using the above equation of motion and considering the magnetic levitation system in the z direction, we choose $x = (z, \dot{z})^T$ as the state variable. Then, the state space equation can be written as:

$$\begin{cases} \mathrm{x(t)} = \mathrm{A_1 x(t)} + \mathrm{B_1 u} \\ \mathrm{y} = \mathrm{C_1 x} + \mathrm{D_1 u} \end{cases}, A_1 = \begin{bmatrix} 0 & 1 \\ \frac{k_z}{m} & 0 \end{bmatrix}, B_1 = \begin{bmatrix} 0 \\ \frac{k_i}{m} \end{bmatrix} \tag{18}$$

$$C_1 = [1 \quad 0] \quad D_1 = 0 \tag{19}$$

Table 1 Parameters of the AMB-flywheel

Item	Value	Unit
Flywheel diameter	0.4	m
Flywheel thickness	0.04	m
Rotor mass(m)	100	Kg
Polar moment of inertia(I_z)	1.114	kg·m^2
Other moment of inertia(I_r)	2.610	kg·m^2
Constant of radial AMB(k_u, k_l)	25.196×10^{-6}	Nm^2/A^2
Constant of axial AMB(k_z)	70.568×10^{-6}	Nm^2/A^2
Distance of upper AMB from center of gravity(L_u)	1.815×10^{-1}	m
Distance of lower AMB from center of gravity(L_l)	3.086×10^{-1}	m
Nominal air gap in radial direction	0.5×10^{-3}	m
Upper nominal air gap in axial direction(z_u)	0.4×10^{-3}	m
Lower nominal air gap in axial direction(z_l)	0.6×10^{-3}	m
Nominal touchdown gap in radial direction	0.2×10^{-3}	m
Nominal touchdown gap in axial direction	0.4×10^{-3}	m
Allowable current	6.0	A

III. SAC ALGORITHM

SAC is a simple yet robust algorithm for unmodeled dynamics [3]. In this algorithm, a plant model of order n_p is described as:

$$\begin{cases} \dot{x}_p = A_p x_p(t) + B_p u(t) \\ y_p(t) = C_p x_p(t) \end{cases} \tag{20}$$

where $x_p(t)$ is the n_p th-order plant state vector, $u(t) \in R^{nj\times1}$ is the system input vector, $y_p(t) \in R^{nj\times1}$ is the system output vector. The plant output $y_p(t)$ is required to asymptotically track the output of the following model y_m.

$$\begin{cases} \dot{x}_m = A_m x_m(t) + B_m u_m(t) \\ y_m(t) = C_m x_m(t) \end{cases} \tag{21}$$

If we let tracking error $e_y(t) = y_m(t) - y_p(t)$, the SAC controller can be defined as:

$$u(t) = k(t)z(t) \tag{22}$$

$$z(t) = [e_y(t), x_m(t), u_m(t)]^T \tag{23}$$

$$k(t) = [k_e, k_x, k_u] \tag{24}$$

Further, $k(t)$ which consists of two parameters, is adaptively adjusted by the following parameter laws:

$$k(t) = k_I(t) + k_p(t) \tag{25}$$

$$\dot{k}_I(t) = \Gamma_I z(t) e_y(t) - \delta(t) k_I(t) \tag{26}$$

$$k_p(t) = \Gamma_p z(t) e_y(t) \tag{27}$$

$$\delta(t) = \frac{\delta_1 e_y(t)^2}{\{\delta_3 + e_y(t)^2\}} + \delta_2 \tag{28}$$

where , δ_1, δ_2, and δ_3 are small positive constants and Γ_I and Γ_p are constant matrices. The SAC structure is shown in Fig.2.

In order to prove the stability of the closed-loop system, the controlled plant is required to be SPR or ASPR. The ASPR conditions are as follows:

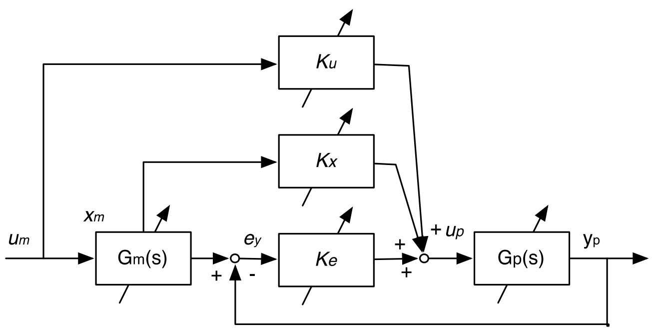

Fig. 2: Block diagram of the SAC scheme

A. The system plant is strictly proper or proper

B. $G_p(s)$ is the minimum-phase

C. $G_p(s)$ has the minimal realization {A, B, C}, where $CB > 0$.

However, since most practical systems do not satisfy the ASPR condition, the ASPR conditions are the fundamental restrictions for practical applications of the output-feedback -based adaptive control.

IV. MULTIPLE-INPUT MULTIPLE-OUTPUT SAC FOR AMB-FLYWHEEL SYSTEM

We consider the application of the proposed method to control the AMB-flywheel system. The AMB-flywheel is a multiple-input multiple-output system with five degrees of freedom. To formulate the design procedure, consider the MIMO flywheel system's transfer function with four DOF in the radial direction:

$$G_p(s) = \begin{bmatrix} g_{11} & g_{12} & g_{13} & g_{14} \\ g_{21} & g_{22} & g_{23} & g_{24} \\ g_{31} & g_{32} & g_{33} & g_{34} \\ g_{41} & g_{42} & g_{43} & g_{44} \end{bmatrix} \tag{29}$$

where each element g_{ij} of $G_p(s)$ is of the form:

$$g_{ij}(s) = \frac{c_p^{ij} s^p + c_{p-1}^{ij} s^{p-1} + \cdots + c_0^{ij}}{B_r^{ij} s^r + B_{r-1}^{ij} s^{r-1} + \cdots + B_0^{ij}} \tag{30}$$

Here, $i, j = 0,1 \cdots, 4$. From the transfer function and root locus of the AMB-flywheel system, it is easy to conclude that none of these transfer functions satisfy the conditions of ASPR. Fig.3 shows the root locus of one element of $G_p(s)$. A PFC should be developed to make the augmented system a minimum-phase system and ensure that it has a relative degree one [4, 6]. In this case, the PFC plant shown in Fig.4 is defined as:

$$R_p(s) = \frac{D}{\tau s + 1} = \frac{10^{-6}}{1000s + 5000} \tag{31}$$

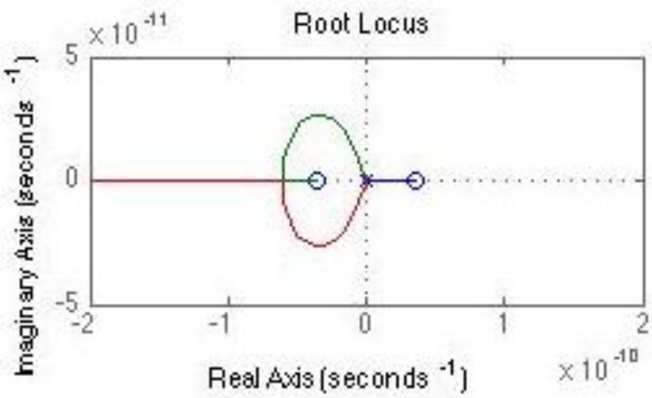

Fig. 3: Root locus for one element of $G_a(s)$

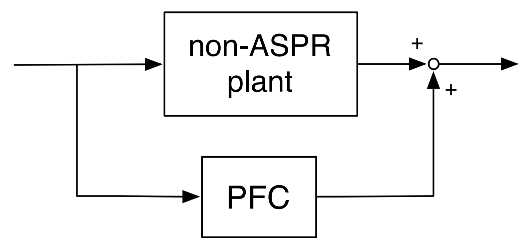

Fig. 4: Block diagram of the augmented plant

Since the AMB-flywheel system is a MIMO system, this PFC plant is added to each element $g_{ij}(s)$ of plant $G_p(s)$. The augmented plant is represented as:

$$G_a(s) = G_p(s) + R_p(s) \tag{32}$$

Augmented measured output:

$$z_p(t) = y_p(t) + r_p(t) \tag{33}$$

Augmented tracking error:

$$e_y(t) = y_m(t) - z_p(t) \tag{34}$$

We design the PFC such that it renders the augmented system to be ASPR. Fig.5 shows the root locus of (34). In this plot, the symbol x shows poles, and the symbol o shows zeros. It is easy to know that the PFC makes the augmented system a minimum-phase system from poles and zeros coordinates, and ensures its relative degree one from (32).

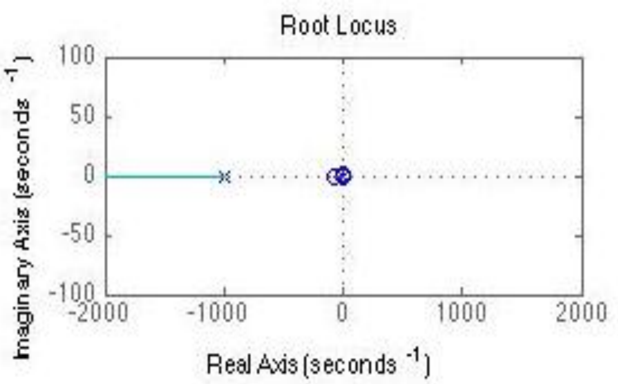

Fig. 5: Root locus for one element of $G_a(s)$

We consider that the AMB-flywheel system it a SISO system in the axial direction. According to the state space (18), the transfer function in the z direction can be written as:

$$G(s) = \frac{K_i / m}{s^2 - K_z / m} \tag{35}$$

It is clearly seen that these transfer functions do not satisfy the conditions of ASPR. Therefore, a PFC should also be developed to make this augmented system a minimum-phase system and ensure its relative degree one.

$$G_{PFC}(s) = \frac{10^{-7}}{K_D s + K_p} = \frac{10^{-7}}{1000s + 50000} \tag{36}$$

$$G_a(s) = G(s) + G_{PFC}(s)$$
$$= \frac{10^{-10}s^2 - (K_i/m)s - (10^{-10}K_z/m + 50K_i/m)}{s^3 + 50s^2 - K_z/m \cdot s - 50K_z/m} \tag{37}$$

This transfer function of the augmented plant has a relative degree one, and the value of the leading coefficient is positive. Analysis of the root locus of $G_a(s)$ confirms that the PFC makes the augmented $G_a(s)$ a minimum-phase system.

The air gap is very small between the rotor of flywheel and touchdown bearing, so AMB controller requires high response speed and small overshoot. In SAC, auto-adjustment of the gain parameters is originally based on the PI adaptive identification rule [5]. Here, for a quicker response and stronger adaptability and robustness characteristics for AMB-flywheel system. The reference model is set as zero, because the flywheel rotor is meant to track the zero-point position in the SAC-D controller. SAC with the derivative rule is shown in Fig.6. The tracking error (34) is adjusted to achieve $\lim_{t\to\infty} e_y(t) = 0$. Hence, the controller can be defined as

$$u_p(t) = k(t)z(t) \tag{38}$$

$$z(t) = e_y(t) \tag{39}$$

$$k(t) = k_I(t) + k_p(t) + k_D \tag{40}$$

$$k_p(t) = \Gamma_p z(t) e_y(t) \tag{41}$$

$$\dot{k}_I(t) = \Gamma_I z(t) e_y(t) - \delta(t) k_I(t) \tag{42}$$

$$k_D = -\frac{de_y(t)}{dt} z(t)^T \Gamma_D \tag{43}$$

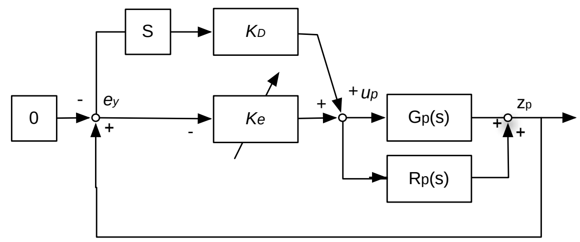

Fig. 6: Block diagram of SAC with derivation action

V. ZERO-BIAS CURRENT MAGNETIC BEARING

Since the AMB-flywheel system is used as a storage device for electrical energy, it is desirable to minimize the energy required for its stabilization control. Zero-bias current magnetic bearings have the potential to reduce power losses because only a single electromagnet of the pair is operational at any time. The switching rule of zero-bias control is defined as:

$$f = f_1 + f_2 \tag{44}$$

$$f = \begin{cases} f_1 \quad (f_2 = 0), \quad if \quad x \geq 0 \\ f_2 \quad (f_1 = 0), \quad other \end{cases} \tag{45}$$

The SAC control input $U = (f_{xu}, f_{xl}, f_{yu}, f_{yl})$ is provided in the form of an attractive force between the electromagnets, but it should be converted into electric current. According to the above equations (44) (45) and (3), the zero-bias mode can be expressed as:

$$\begin{cases} f_{xu} \geq 0 \quad i_1 = (|X_0| - X_u)\sqrt{\dfrac{f_{xu}}{k_u}}, i_3 = 0 \\ f_{xu} < 0 \quad i_1 = 0, i_3 = (|X_0| + X_u)\sqrt{\dfrac{-f_{xu}}{k_u}} \end{cases} \tag{46}$$

$$\begin{cases} f_{xl} \geq 0 \quad i_5 = (|X_0| - X_l)\sqrt{\dfrac{f_{xl}}{k_u}}, i_7 = 0 \\ f_{xl} < 0 \quad i_5 = 0, i_7 = (|X_0| + X_l)\sqrt{\dfrac{-f_{xl}}{k_l}} \end{cases} \tag{47}$$

The zero-bias modes of other electromagnet pairs follow the same form.

VI. CONFIGURATION OF TEST SYSTEM

The flywheel system designed for a five-axis controlled AMB system and the electric vehicle equipped with the designed flywheel system are shown in Fig. 7.

Fig. 7: Overview of AMB-flywheel and EV

Fig. 8 shows the overview of the entire control system. The control system consists of five components, including the flywheel, the power source, amplifier, and a compact PCI (cPCI) platform computer system.

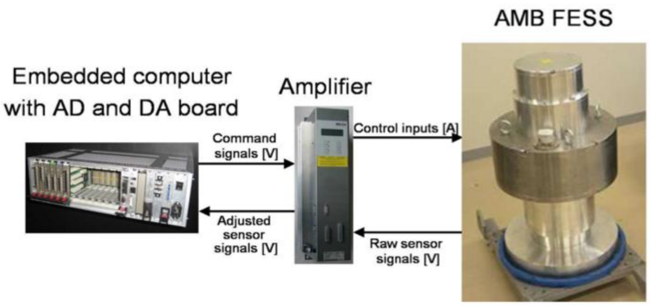

Fig. 8: Configuration of AMB-flywheel system

VII. SIMULATION

A simulation model was constructed using the transformed state space equations. The response to a 0.1 mm initial step input was injected into the upper rotor in the x direction in order to obtain a step response. Fig.9 shows the step response of the displacement as a control output, which traces the step reference signal rapidly and stably. The rotor levitates perfectly toward the center point by SAC.

The control currents i_1 and i_3 for one electromagnet of the pair are shown in Fig.10. Since the zero-bias control is used for this AMB-flywheel system, i_1 and i_3 follow the zero-bias mode rule expressed in (46) and (47). The control currents converge to zero after the rotor is suspended at the center position.

In this section, we present the analysis of the influence of external disturbances from the EV driving on the road about the AMB-flywheel system. A real disturbance is used in the simulation program for testing the stability of the SAC controller in the radial direction (x and y directions) of the AMB-flywheel system. The disturbance data are collected by the acceleration sensor under two road conditions: driving in the campus and driving in the city.

These acceleration data are added to the simulation model of the flywheel as disturbance. Fig.11 shows the measured acceleration data in the driving experiments. The maximum acceleration value is about 0.4g.

Fig.12 shows the displacement of the flywheel rotor under this disturbance. In this case, the displacement results demonstrate that the SAC controller can stabilize levitation of the AMB system without any touchdown. The gains of SAC with a D controller are shown in Fig.13. It can be seen that the gain fluctuations can respond rapidly under the real disturbance.

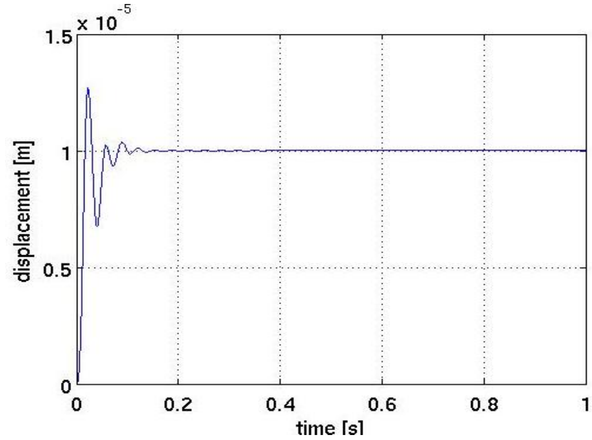

Fig. 9: Step response of the flywheel rotor

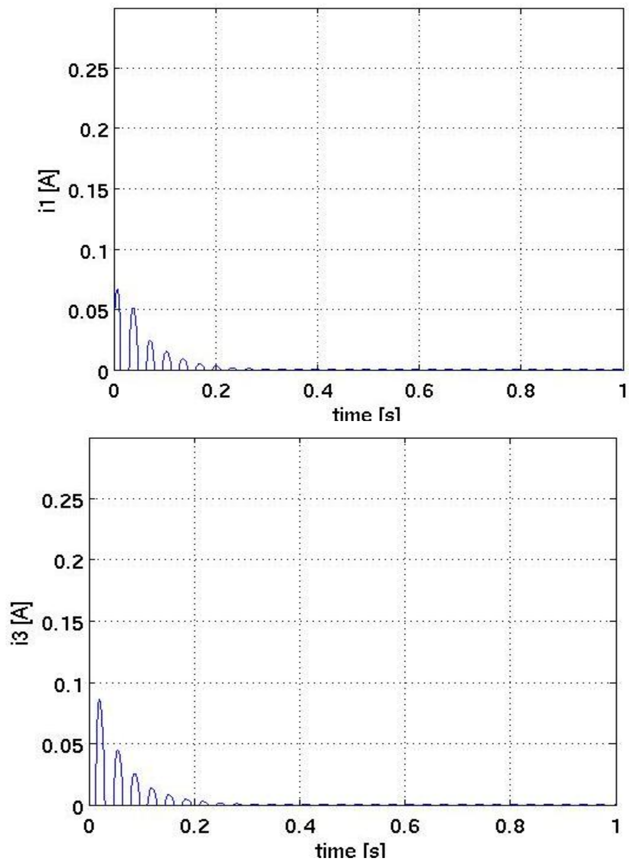

Fig. 10: Control currents i1 and i3

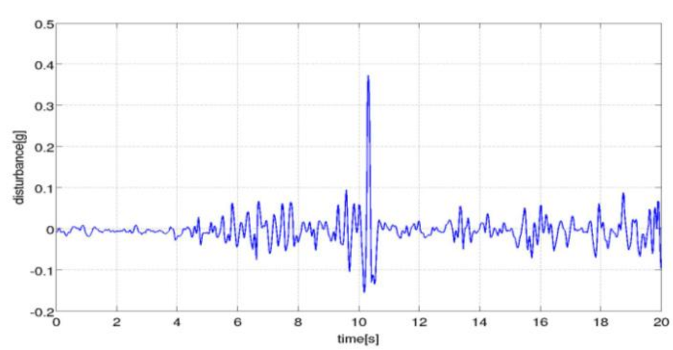

Fig. 11: Measured acceleration data for driving in the city

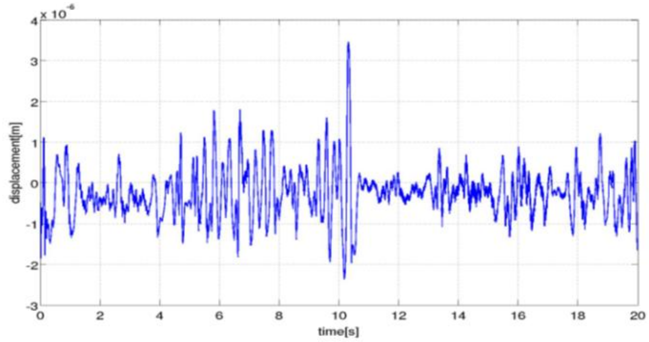

Fig. 12: Displacement result for the upper x direction

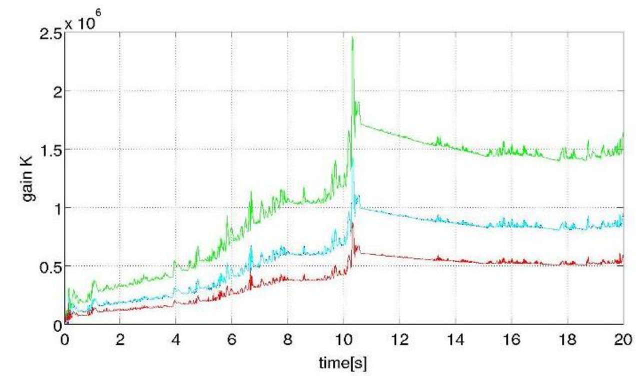

(a) Gain k_p

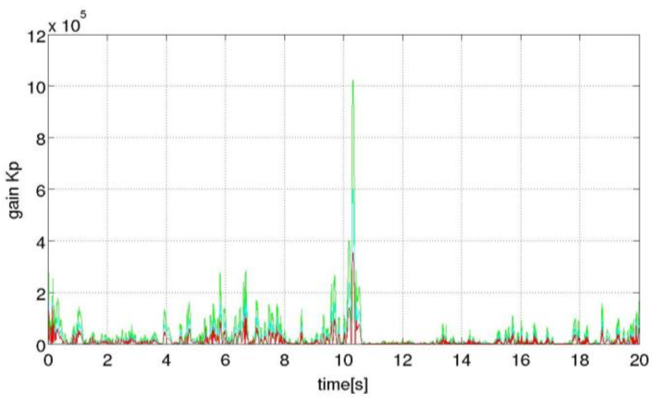

(b) Gain k

Fig. 13: Gain fluctuation under applied disturbance

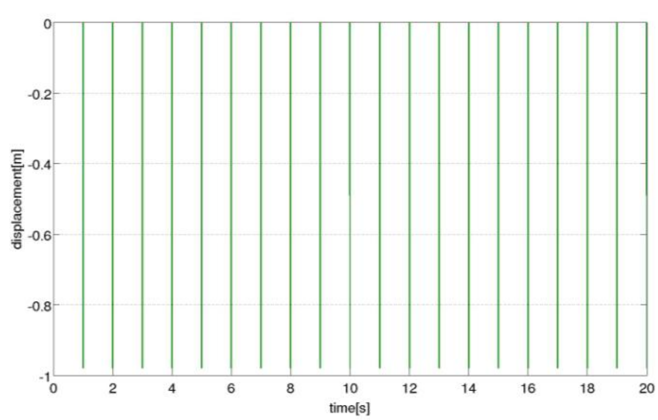

Fig. 14: Pulse disturbance

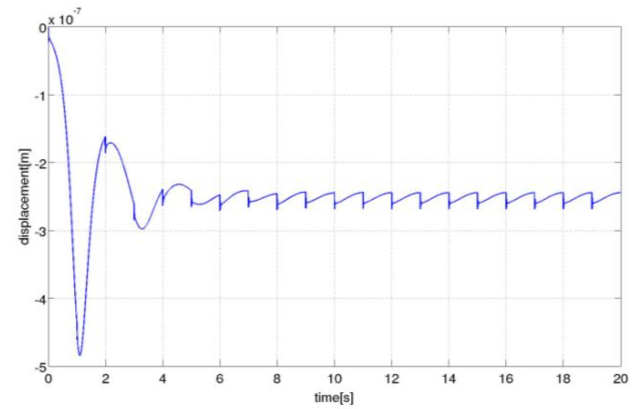

Fig. 15: Displacement in z direction under disturbance

Fig. 14 shows a 4 seconds period and 1 G disturbance in z direction. Fig.15 shows the displacement in the z direction under the pulse disturbance shown in Fig.14. The displacement results show that the SAC controller can stabilize levitation of the AMB system in the z direction under a 1G pulse disturbance without any touchdown.

VIII. EXPERIMENT

Experiments were performed on SAC with the zero-bias modes. Fig.16 shows the time history of the flywheel rotor displacement in the radial direction. The displacements were used to evaluate the control performance. The control program began after 1.4 s. The control gains of SAC can be explained using (38)-(43), the gains k and k_i are shown in Fig. 17.

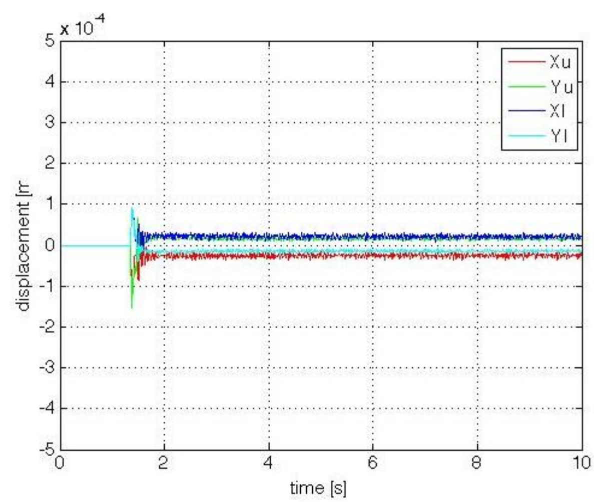

Fig. 16: Time history response of flywheel rotor

The control currents in the x direction of the upper electromagnets during the levitation experiment are shown in Fig. 18. As seen in the figure, the maximum current is 1.5A for a rotor levitating from its initial position to the center position of the flywheel, and the stability suspension control current is 0.5A. The control current also satisfies the condition of the zero-bias mode. The simulation result of the step response is shown in Fig. 19; this figure also presents a comparison between the results of the displacement determined in the experiment and the simulation. Fig.20 shows the orbits for the upper and lower sides of the flywheel rotor. Fig.21 shows the time history of the flywheel rotor displacement in the *z* direction.

The control currents in the *x* direction of the upper electromagnets during the levitation experiment are shown in Fig.18. As seen in the figure, the maximum current is 1.5A for a rotor levitating from its initial position to the center position of the flywheel, and the stability suspension control current is 0.5A. The control current also satisfies the condition of the zero-bias mode. The simulation result of the step response is shown in Fig.19; this figure also presents a comparison between the results of the displacement determined in the experiment and the simulation. Fig.20 shows the orbits for the upper and lower sides of the flywheel rotor. Fig.21 shows the time history of the flywheel rotor displacement in the *z* direction.

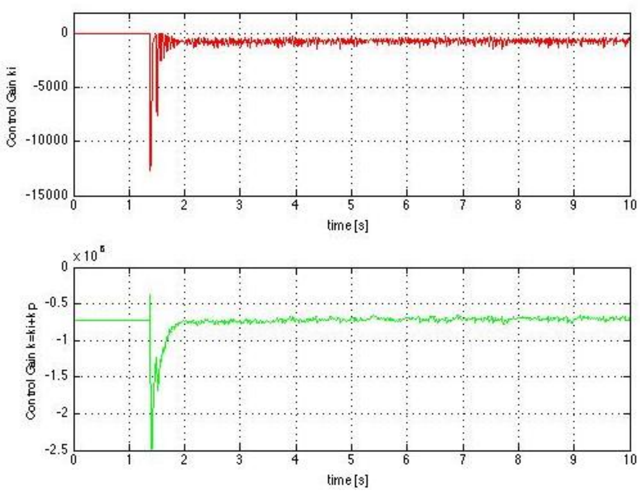

Fig. 17: SAC control gains k and k_i

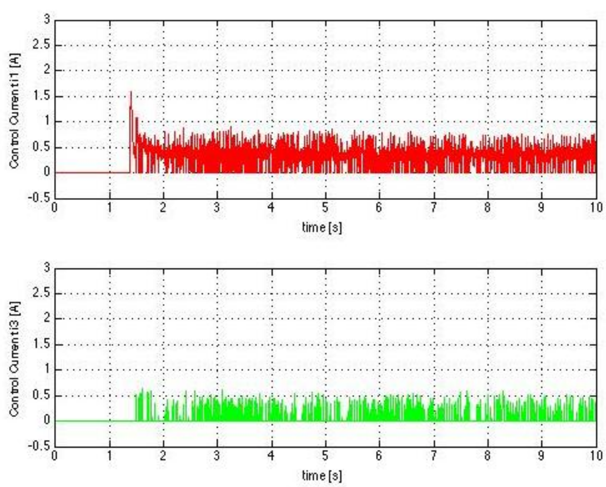

(a) Overview of control current

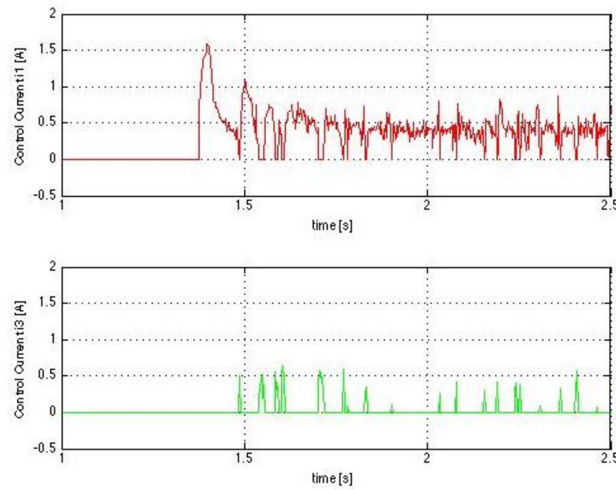

(b) Extended control current

Fig. 18: Control currents

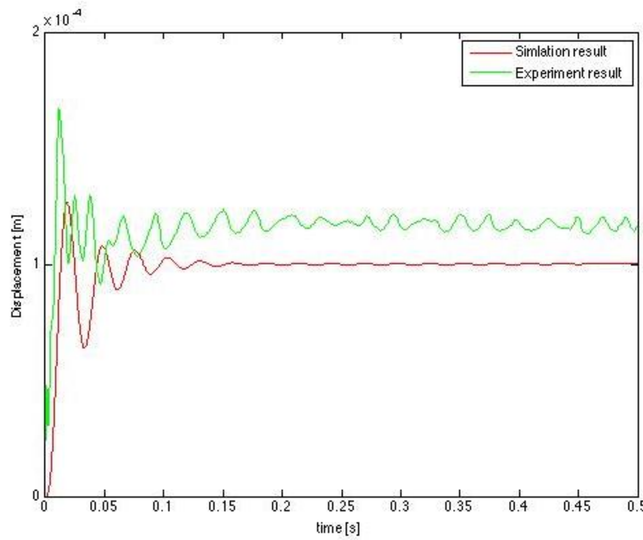

Fig. 19: Comparison of displacements determined by simulation and experiment

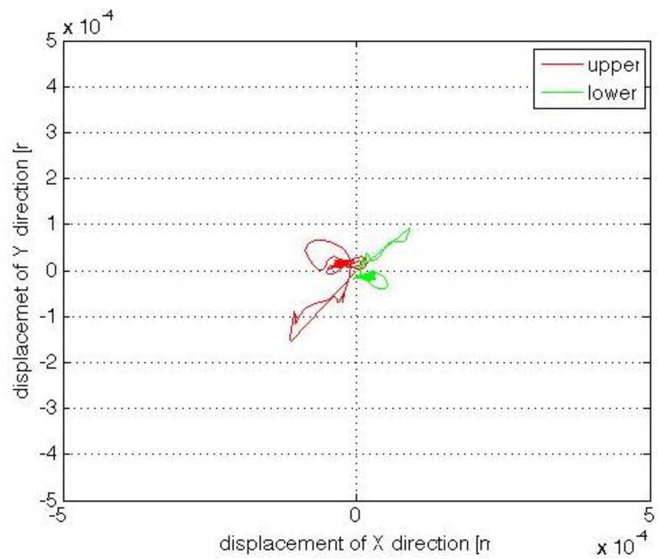

Fig. 20: Orbits for upper and lower side's rotor

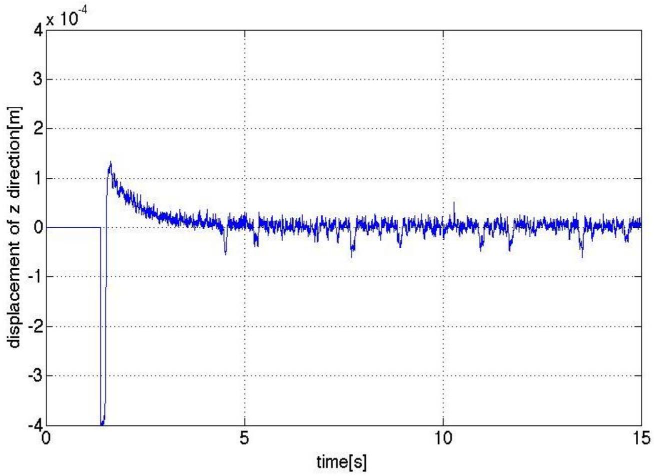

Fig. 21: Displacement in z direction

IX. CONCLUSIONS

In this study, a simple adaptive control (SAC) was proposed for application to AMB-flywheel system and control performance was improved by combining SAC with a D controller. In the proposed approach, the unmeasured states of the bearing system are eliminated by a model that adopts SAC.

SAC was successfully applied to vertically designed five-axis controlled AMB-flywheel systems. The experimental results were found to satisfy the requirements of the AMB-flywheel system. The zero-bias mode did not deteriorate the stability of the control system; further, energy consumption in this mode was low.

REFERENCES

[1] Selim Sivrioglu, Muneharu Saigo, and Kenzo Nonami. Adaptive backstepping control design for a flywheel zero-bias AMB System. IEEE, Control Applications. Vol.2, PP. 1106–1111, 2003.

[2] Sirish Shah, Zenta Iwai, and Ikuro Mizumoto. Simple adaptive control of processes with time-delay. J. Pro. Cont. Vol.7, No. 6, PP. 439–449, 1997.

[3] Howard Kaufman, Itzhak Barkana, and Kenneth Sobel. Direct Adaptive Control Algorithms Theory and Applications-2 Ed., Springer Verlag New York, 1997.

[4] Ikuro Mizumoto and Hiroki Tanaka. Model free design of PFC for adaptive output feedback control and application to a control of magnetic levitation system. 2010 IEEE International Conference on System and Control, Yokohama, Japan. PP. 35–40. 8–10 Sept., 2010.

[5] Budi Rachmanto and Kenzo Nonami. A study on AMB-flywheel powered electric vehicle. Journal of System Design and Dynamics. Vol.3, No. 4, PP. 659–670, 2009.

[6] Goo-Jong Jeong, In-Hyuk Kim, and Young-Ik Son. Application of simple adaptive control to a DC/DC boost converter with load variation. ICCAS-SICE. Fukuoka. P. 1747, 2009.